

IMPROVED BOW SHOCK MODELS FOR HERBIG-HARO OBJECTS: APPLICATION TO HH 2A'

JOHN C. RAYMOND,^{1,3} PATRICK HARTIGAN,^{2,3} AND LEE HARTMANN^{1,3}

Received 1987 June 18; accepted 1987 August 18

ABSTRACT

We present an improved version of the bow shock theory previously applied to Herbig-Haro objects. The modifications provide a more accurate calculation of the ionization state of material entering the bow shock. The revised preionization does not drastically affect the emission-line predictions for a 200 km s^{-1} bow shock model, though the effects will be more severe for slower shock velocities. The line profiles of the new models resemble the observed profiles somewhat more closely, and the relative emission-line intensities typically differ by 30% from those predicted by the older models. The models agree well with new *IUE* spectra and existing optical data for HH 2A'.

Subject headings: shock waves — stars: pre-main-sequence — ultraviolet — spectra

I. INTRODUCTION

The intensity ratios of the optical emission lines of Herbig-Haro objects first suggested shock excitation (Schwartz 1975), and plane-parallel models of radiative shocks matched their intensities reasonably well (Dopita 1978; Raymond 1979). However, the first *IUE* spectrum of an HH object showed ultraviolet emission lines far stronger than would be predicted for the slow shock velocities inferred from the optical line ratios (Ortolani and D'Odorico 1980). Bow shock models for HH objects, first suggested by Schwartz (1978), have proved quite successful in explaining both the overall spectra and the line profiles of HH object knots (Hartmann and Raymond 1984; Choe, Böhm, and Solf 1985; Raga and Böhm 1985; Hartigan, Raymond, and Hartmann 1987, hereafter HRH). The combination of strong UV lines and modest [O III] emission arises naturally from the range of effective shock velocities present in a bow shock, and the tangential component of the gas velocity directly produces the large observed line widths. The bow shock hypothesis also reconciles the observed proper motions with the spectra and line profiles.

While the bow shock models of HRH match both the line profiles and the relative line intensities remarkably well, their treatment of the preshock ionization is not entirely self-consistent. The models approximate the bow shock as a set of annuli, with the emission from each annulus given by a plane-parallel shock model with a preshock ionization state determined by the radiation from the shock in that annulus (hereafter "local equilibrium"). However, the severe curvature of the bow shock means that gas approaching one segment of the bow shock is exposed to the radiation field from parts of the bow shock having different effective shock velocities.

We have computed the preshock ionization state as a function of distance from the axis for several bow shock models. As expected, the preshock gas is less ionized near the bow shock tip and more ionized in the wings than it would be with local equilibrium preionization. A set of plane-parallel models with appropriate preionization was computed and used to predict

the line intensities and profiles for a 200 km s^{-1} bow shock. The predictions are not drastically altered by the revised preionization, but the line profiles are somewhat closer to those observed.

The new model is compared with *IUE* and optical observations of HH 2A', an especially interesting object because of its recent appearance and its brightness, high excitation, low reddening, and broad, asymmetric line profiles.

II. MODEL CALCULATIONS

Hartmann and Raymond (1984) and HRH approximated the emission from a bow shock by a set of planar shocks having effective velocities, v_{eff} , given by the normal component of the velocity at each point along the bow shock. The emission spectrum of a planar shock depends on the ionization state of the gas entering the shock, and the bow shock models were based on either the assumption of complete preionization or the assumption of local equilibrium preionization. In the equilibrium assumption, which generally predicted spectra in better agreement with those observed, the preshock gas is exposed to the ionizing radiation produced by the shock, and an equilibrium is reached between the number of ionizing photons produced in the shock and the number of ionized atoms entering it (Shull and McKee 1979). The transition between essentially neutral and essentially ionized preshock gas occurs over a narrow velocity range, $90 < v_s < 120 \text{ km s}^{-1}$, because of the efficiency of neutral hydrogen in cooling the gas by means of (nonionizing) Lyman line emission.

The assumption of local equilibrium preionization is appropriate provided that the shock maintains a constant speed long enough to attain the steady state, and the shock is close enough to planar that the upstream flow is not exposed to radiation from regions of different v_{eff} . The first condition is met if the cooling time of the shocked gas is less than the ages of the knots. For the knots of HH 1 and HH 2, which have been observed for 30 years or more, this requires a preshock density, greater than about 200 cm^{-3} . The second condition depends on both the bow shock curvature and n_0 . The effective shock speed changes significantly over a scale $\sim 0.1R_0$, where R_0 is the radius of the cloud producing the bow shock. If $0.1R_0 n_0$ is much greater than 10^{18} cm^{-2} , the opacity of the preshock gas will effectively isolate the flow from radiation produced at different effective shock velocities.

¹ Harvard-Smithsonian Center for Astrophysics.

² Department of Planetary Sciences, University of Arizona.

³ Guest Observer with the *International Ultraviolet Explorer* satellite, which is jointly operated by the US National Aeronautics and Space Administration, the Science and Engineering Research Council of the UK, and the European Space Agency.

A treatment of the ionization ahead of a bow shock involves two-dimensional radiative transfer and nonequilibrium ionization. It is unpleasantly nonlinear, since the flux of ionizing radiation produced at each point of the bow shock depends on the ionization state of the gas it encounters. Considering the exploratory nature of the calculation and the approximations involved in the bow shock models themselves, we are prepared to make some severe approximations.

The calculation proceeds by iteration, starting with an initially neutral preshock flow on a grid of 100 cells along the axis by 20 annuli. For each annulus the effective shock velocity, v_{eff} , is found from the modified Raga (1986) bow shock shape preferred by HRH, with $R_0 = 10^{16}$ cm and $n_0 = 100 \text{ cm}^{-3}$. From v_{eff} and the ionization state of gas entering the shock, we compute the equivalent shock velocity for an ionized medium following the prescription of Cox and Raymond (1985). This equivalent shock velocity, v_i , is used to find the number of ionizing photons which travel upstream through the shock front for each atom which passes through it. We interpolate among the ionizing photon fluxes listed in Table 1, which are based on the models listed in Table 2 of HRH. The energy of each ionizing photon is assumed to be 16 eV. For each iteration, the ionizing radiation from each annulus propagates upstream, with Lyman continuum absorption and geometrical dilution taken into account. The geometrical factors are further simplified by treating the bow shock as though it were flattened into a plane. The radiation field during each iteration is used to compute a revised ionization state for the next iteration. The time-dependent ionization calculation for hydrogen flowing toward the bow shock assumes a constant temperature of 5000 K and the "on-the-spot" approximation for absorption of photons emitted by recombinations to the ground state. The ionization state in the cell at the shock is used to revise v_i , and the ionization state of the upstream gas is used to compute Lyman continuum absorption in the next iteration.

These approximations tend to predict preshock ionization structures unrealistically close to local equilibrium preionization. Many of the photons are more energetic than 16 eV, and they penetrate through the upstream gas more effectively than the 16 eV photons assumed. The artificially flattened geometry reduces the time that gas approaching the bow shock wings is exposed to the ionizing radiation from the bow shock tip, while at the same time it underestimates the dilution of radiation produced in the outer annuli of the bow shock as seen by gas approaching the tip. A more detailed treatment would compute the diffuse hydrogen recombination radiation field, instead of assuming on-the-spot reabsorption of these photons. This would reduce the number of ionized atoms entering the shock, but extend the ionization farther from the axis.

Figure 1 displays the results. The hydrogen neutral fractions for gas encountering 150, 200, 250, and 300 km s^{-1} bow shocks are shown plotted against distance from the axis. The neutral

fractions for equilibrium preionization are shown by the dashed lines, and v_{eff}/v is indicated by the dotted lines. Even though the model underestimates the departures from local equilibrium preionization, the gas is significantly underionized at the bow shock tip, while even in the very small v_{eff} regions in the bow shock wings the gas is significantly ionized.

Planar shock models were computed as described in HRH using the hydrogen ionization states computed for the 200 km s^{-1} model. This velocity is near the average of the bow shock velocities derived for HH 2A' from the profiles of six lines (HRH, Table 4). The balance between He^0 and He^+ was assumed to be the same as the hydrogen neutral-to-ionized ratio, and it was assumed that helium was significantly doubly ionized only for $v_{\text{eff}} > 180 \text{ km s}^{-1}$. This is not a very reliable approximation, but a much more sophisticated calculation would be required to predict the helium ionization state accurately. The helium ionization state can significantly affect the cooling of the shocked gas and the emergent spectrum, but these effects are somewhat less than the effects of the hydrogen ionization we are treating. The plane-parallel shock models include a radiation transfer parameter R_{max} related to the ratio of the transverse extent of the shock to the cooling length of the shocked gas (Cox 1972). HRH used $R_{\text{max}} = 1.0$, corresponding to a transverse extent about 5 times the cooling length, while the present models used $R_{\text{max}} = 3.0$, corresponding to a ratio of about 40. The larger value of R_{max} increases the recombination part of the $\text{H}\beta$ emission and the emission of the low ionization stages by something like 10%. For HH 2A' in particular, the $R_{\text{max}} = 1$ models are probably more appropriate. The line intensities given by the planar models were then entered into the codes described by HRH to predict the emission-line fluxes and line profiles from the bow shock.

The planar shock models were computed with $n_0 = 1000 \text{ cm}^{-3}$, while the preionization calculation assumed $n_0 = 100 \text{ cm}^{-3}$. Since the ionization structure scales with $n_0 R_0$, the calculation is self-consistent for $R_0 = 10^{15}$ cm. However, as discussed above, the approximations involved in the preionization calculation tend to underestimate the departure from equilibrium preionization, and the computed values are probably more appropriate for $R_0 = 3 \times 10^{15}$ cm. In the next section we will compare the predictions with observations of HH 2A', whose apparent diameter suggests $R_0 \sim 7 \times 10^{15}$ cm. The choice of $n_0 = 1000 \text{ cm}^{-3}$ therefore gives an idea of the maximum likely effects of departures from equilibrium preionization.

There is a second reason for choosing $n_0 = 1000 \text{ cm}^{-3}$ for the models. HRH found that a preshock density this large is needed to account for the $\text{H}\beta$ luminosity observed for HH 2H, the luminosity being simply proportional to n_0 . However, the $[\text{O III}] \lambda 3227$ doublet is suppressed at high densities, and the $n_0 = 1000$ model predicted an $[\text{O III}]/\text{H}\beta$ ratio only 40% as large as observed. The luminosity and $[\text{O III}]/\text{H}\beta$ ratio of HH 2A' present similar difficulties. HRH used a preliminary version of the present preionization calculation with the techniques of Cox and Raymond (1985) to estimate the line ratios which the present calculation would predict. In particular, we predicted a 50% increase in $[\text{O III}]/\text{H}\beta$, which would alleviate the difficulty with the high n_0 model. Unfortunately, the increase turns out to be only 10%, owing to a larger increase in the $\text{H}\beta$ flux than anticipated and higher electron densities in the bow shock wings. Had we used $R_{\text{max}} = 1$, the increase would have been about 20%.

Table 2 shows the spectrum predicted by the model, along

TABLE 1
IONIZING PHOTONS PER ATOM

V	Photons	V	Photons	V	Photons
20.....	0.03	120.....	1.18	220.....	2.75
40.....	0.12	140.....	1.90	240.....	2.91
60.....	0.20	160.....	2.21	260.....	3.03
80.....	0.37	180.....	2.63	280.....	3.06
100.....	0.67	200.....	2.69	300.....	2.75

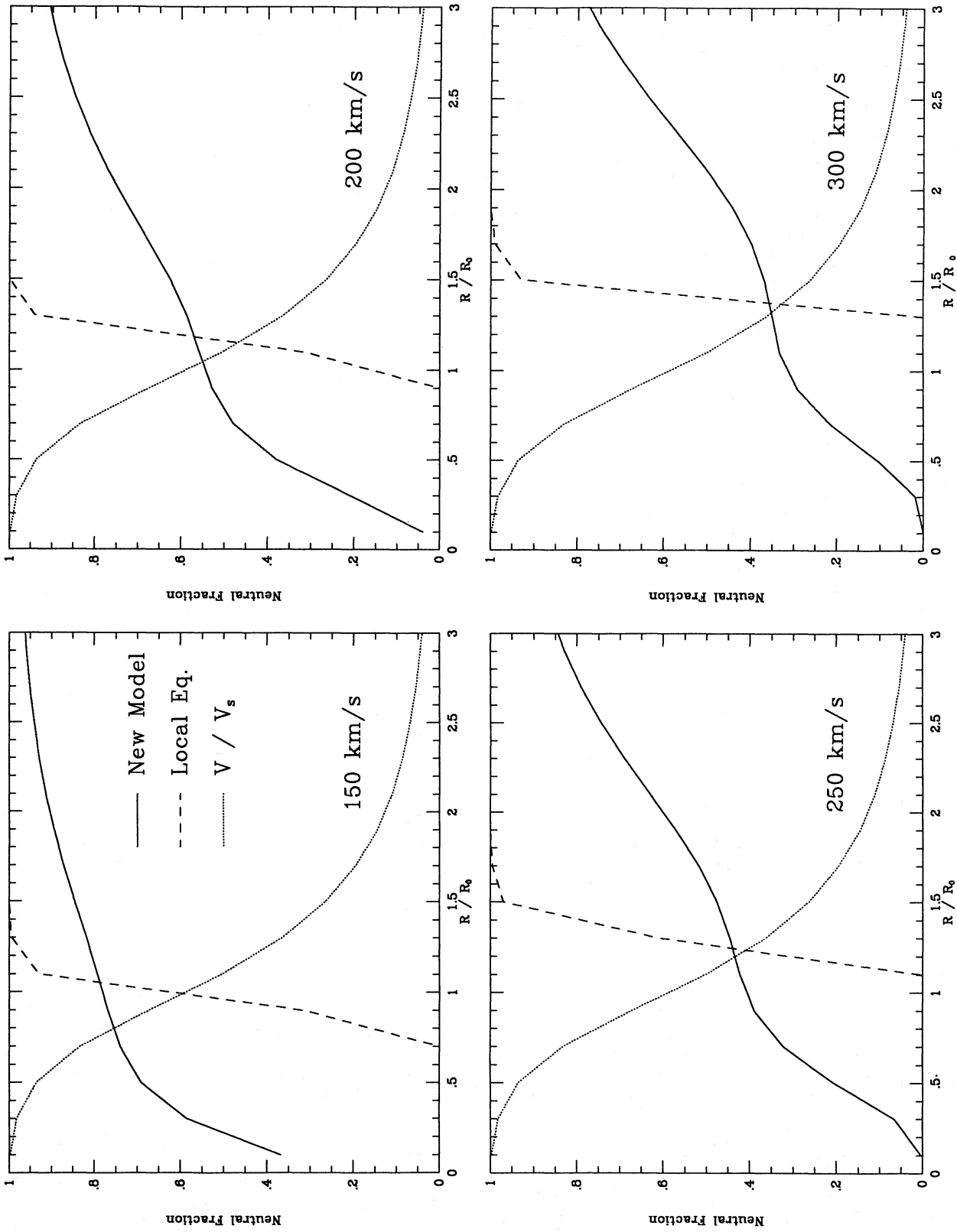


FIG. 1.—Neutral fraction of hydrogen entering the shock front as a function of normalized distance from the axis (R/R_0) for 150, 200, 250, and 300 km s^{-1} bow shocks. The current model is shown as the solid line, and the local equilibrium model as the dashed line. The ratio of the normal component of the velocity to the bow shock velocity at each radius is indicated by the dotted line.

TABLE 2
OBSERVED, DEREDDENED, AND PREDICTED LINE INTENSITIES

Line	F_{obs}	$F_{0.11}$	$F_{0.37}$	HRH Model 5	New Model
N v $\lambda 1240$	209	146
C II $\lambda 1335$	15	17	22	172	122
O IV], Si IV $\lambda 1400$	43	48	61	220	146
C IV $\lambda 1550$	331	370	477	665	504
O III] $\lambda 1662$	123	92
Si III] $\lambda 1891$	87	97	124	126	92
C III] $\lambda 1909$	246	271	351	264	206
C II] $\lambda 2325$	199	176
Mg II $\lambda 2800$	282	359
[O II] $\lambda 3727$	149	165	211	80	87
[Ne III] $\lambda 3868$	10	11	14	40	43
[S II] $\lambda 4070$	62	67	77	108	114
[Fe III] $\lambda 4658$	8	8	9	7	8
H β	100	100	100	100	100
[O III] $\lambda 5007$	119	116	109	203	172
[N I] $\lambda 5200$	6	6	6	18	6
[O I] $\lambda 6300$	220	195	147	204	170
H α	622	546	401	312	296
[N II] $\lambda 6584$	151	132	97	87	84
[S II] $\lambda 6727$	129	112	81	73	60
[O II], Ca II] $\lambda 7320$	146	124	84	124	115
[Fe II] $\lambda 8617$	40	33	20	16	15
[C I] $\lambda 9848$	36	28	16	155	110
Two-photon emission	5130	5710	7420	2110	1750
H β^a	0.691	1.02	2.59	1.21	1.46

^a H β flux in units of 10^{-13} ergs cm $^{-2}$ s $^{-1}$, with the model predictions scaled to $R_0 = 10^{16}$ cm and a distance of 500 pc.

with HRH model 5, the model with the same bow shock parameters and local equilibrium preionization. The predicted emission-line profiles are shown in Figure 2.

III. OBSERVATIONS

Two short-wavelength exposures of HH 2A' were obtained with *IUE* on 1986 December 8 and 10. The spacecraft was offset from SAO 132384 ($\alpha_{1950} = 5^{\text{h}}35^{\text{m}}21^{\text{s}}.109$, $\delta_{1950} = -6^{\circ}44'13''$) to the position of HH 2A' given by Herbig and Jones (1981) ($\alpha_{1950} = 5^{\text{h}}33^{\text{m}}59^{\text{s}}.44$, $\delta_{1950} = -6^{\circ}48'59''$). The first image, SWP 29835 (400 minute exposure), showed the knot of bright emission about 3" from the center of the *IUE* Large Aperture along the direction perpendicular to the dispersion. The blind offset was rather long, and a displacement along the dispersion direction comparable to the displacement perpendicular to the dispersion direction would place the emission knot at the edge of the aperture, reducing the apparent flux. Therefore, a second SWP exposure was obtained (SWP 29845, 390 minutes) using the same offset star and offset position. This time the emission knot was centered. Comparison of the guide-star positions shows that the displacement between the two exposures was almost entirely perpendicular to the dispersion direction. Since the fluxes measured from the two exposures agree, we use the average of the two measurements, and we use the difference between them to estimate the uncertainty.

While the C III] $\lambda 1909$ and C IV $\lambda 1549$ lines can be seen quite clearly in the original IUESIPS extended source reductions, the weaker lines are nearly lost in the noise. Therefore, we have used the line-by-line files to extract the 12 lines ($\sim 12''$) from each exposure which contain $\sim 90\%$ of the C IV and C III] total fluxes in the Large Aperture. The IUESIPS and central region spectra are shown in Figure 3. The fluxes presented in Table 2 are the C III] and C IV fluxes measured from the IUESIPS

reductions, with the weaker lines given by the ratios to the C III] and C IV lines as measured from the central line spectra. The uncertainties in the intensities, dominated by the uncertainty in continuum subtraction, are about 20% for C IV and C III] and at least 50% for the other lines.

For comparison with the model calculations, we need a spectrum covering the full optical-ultraviolet range. This is difficult to obtain because of uncertainties in the absolute calibration of the optical observations and the reddening correction. Hartmann and Raymond (1984) presented an optical spectrum of HH 2A' obtained with the Multiple Mirror Telescope (MMT) spectrograph. The 2" aperture used for that observation is about equal to the apparent size of HH 2A', so the flux from the whole knot may be somewhat greater than that given by Hartmann and Raymond (1984). Brugel, Böhm, and Mannery (1981) observed HH 2A with a 3"6 aperture. The distinction between HH 2A and HH 2A' is somewhat unclear. Herbig and Jones (1981) report that HH 2A faded in the mid 1950s, about the same time that HH 2A' appeared 1" away. The relative line strengths given by Brugel, Böhm, and Mannery are quite similar to those obtained for HH 2A' by Hartmann and Raymond, but the absolute fluxes are about only half as great. One possible interpretation of this discrepancy is that the Hartmann and Raymond flux is a factor of 2 overestimate, since they did not claim higher accuracy. It is also possible that HH 2A' was at the edge of the aperture used by Brugel, Böhm, and Mannery, or that the knot brightened over the 3 years between the two observations. Here we combine the measured *IUE* fluxes, which have absolute calibration uncertainties of around 10%, with the Hartmann and Raymond (1984) optical fluxes, and we will discuss below how the interpretation changes if the Brugel, Böhm, and Mannery (1981) absolute flux is adopted. For lines outside the 4000–7000 Å range observed by Hartmann and Raymond (1984), we

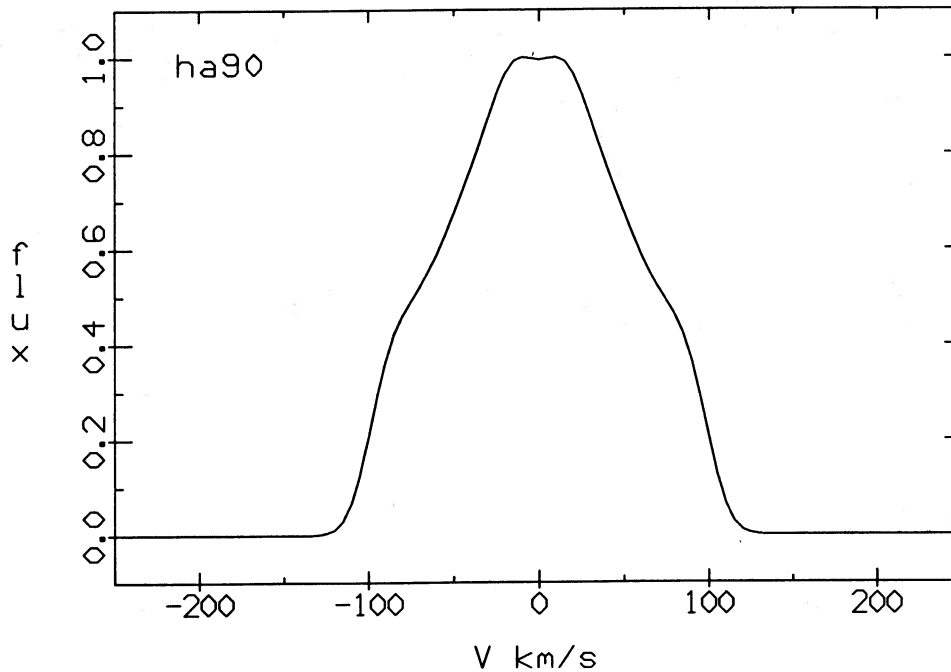


FIG. 2a

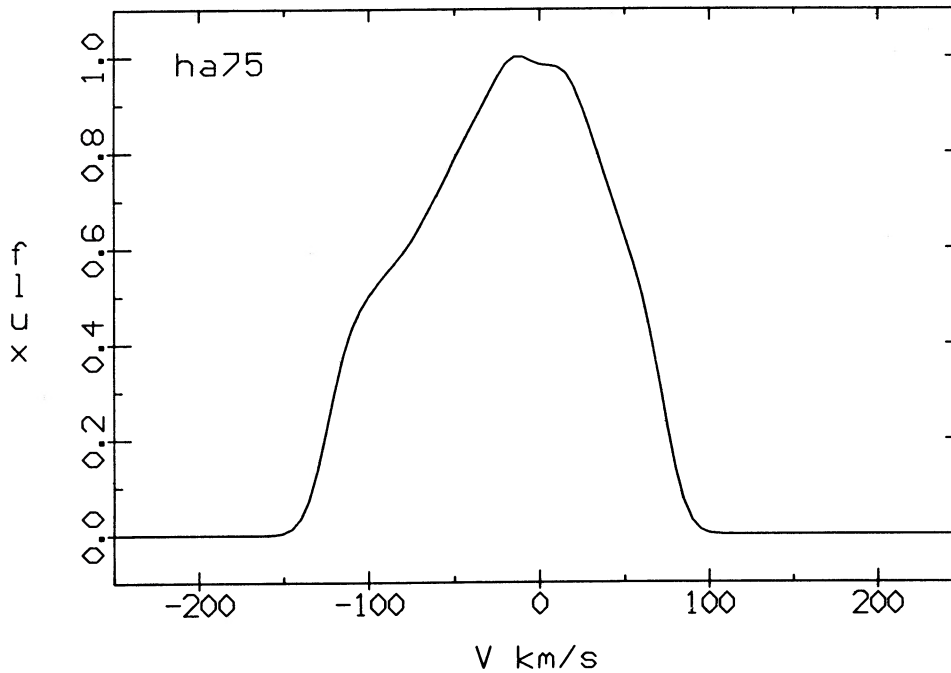


FIG. 2b

FIG. 2.—(a) $H\alpha$ line profile predicted for the 200 km s^{-1} bow shock seen at 90° as inferred by HRH. (b) Same as (a), for 75° . (c) Same as (a) for 60° . (d) Same as (a) for 30° . (e) Predicted $[O \text{ II}]$ profile for 75° . (f) Predicted $[O \text{ III}]$ profile for 75° .

use the ratios to $H\beta$ given by Brugel, Böhm, and Mannery (1981). All these uncertainties will prevent us from drawing any strong conclusions from the relative strengths of UV and optical emission, and the discussion below will be based mostly on ratios of lines not too different in wavelength.

The reddening correction presents another severe problem. Brugel, Böhm, and Mannery (1981) derived $E(B-V) = 0.37$ from the $[S \text{ II}] I(4070)/I(10326)$ ratio of HH 2A. Hartmann and

Raymond (1984) found $E(B-V) = 0.11$ for HH 2A' from comparison of $I(4070)/I(6717 + 6731)$ with $I(6717)/I(6731)$, a method which depends on several collisional rate coefficients and radiative transition probabilities, as well as on the temperature of the $[S \text{ II}]$ emitting region given by the shock models. Table 2 shows the observed line ratios and the ratios corrected for color excesses of 0.11 and 0.37 using the θ^2 Ori reddening curve of Bohlin and Savage (1981) favored by Böhm,

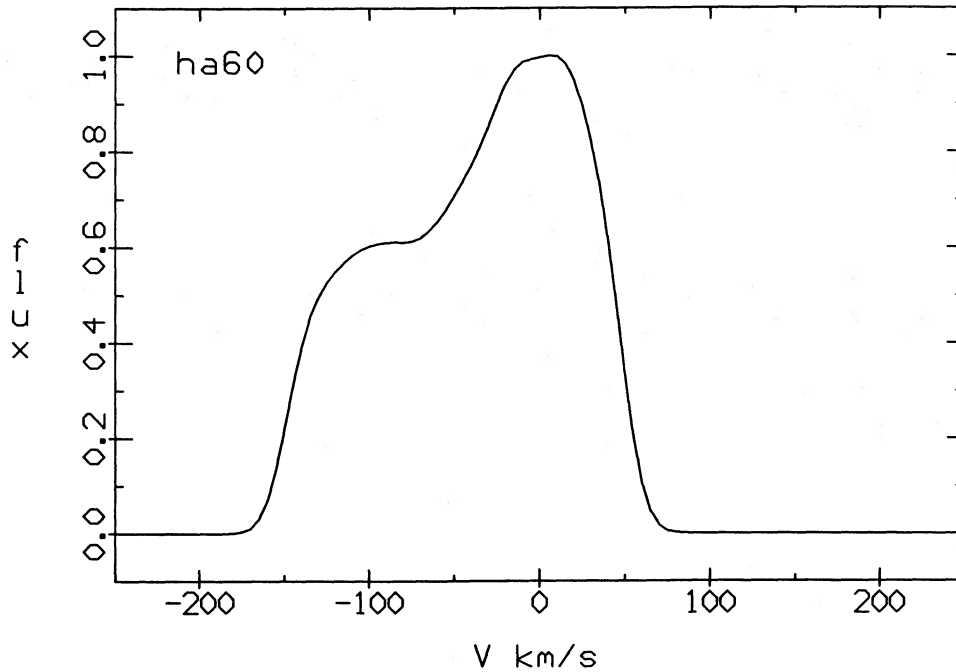


FIG. 2c

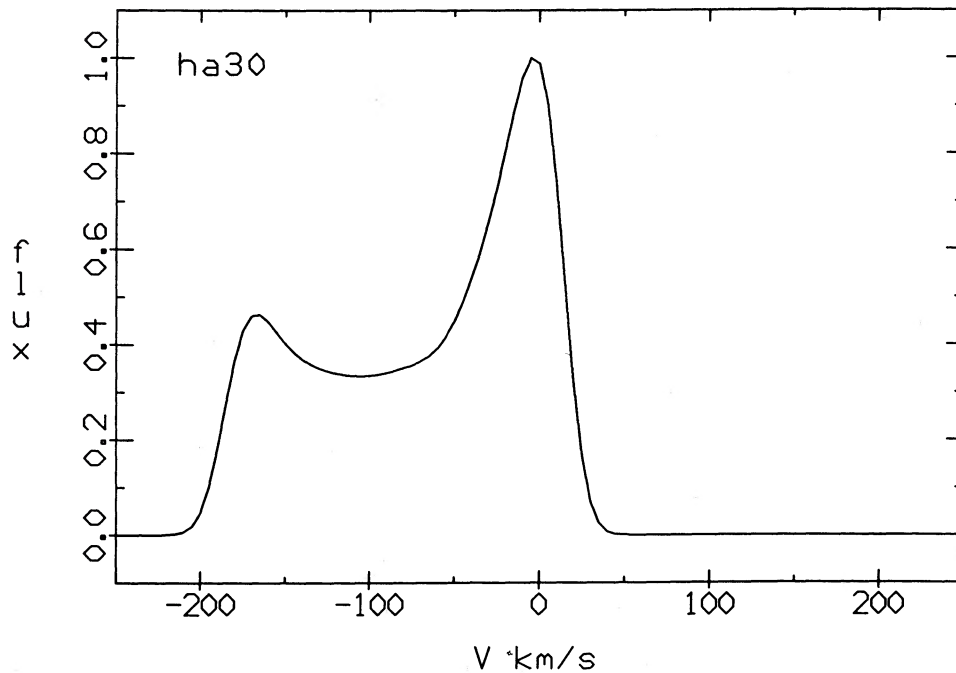


FIG. 2d

Böhm-Vitense, and Cardelli (1982). If we had used the average Galactic extinction law, the UV fluxes corrected for $E(B-V) = 0.11$ would be about equal to those corrected for $E(B-V) = 0.37$ with the θ^2 Ori extinction, and those corrected for $E(B-V) = 0.37$ would be about a factor of 3 higher.

The continua of HH objects are generally attributed to hydrogen two-photon emission (Dopita, Binette, and Schwartz 1982; Brugel, Shull, and Seab 1982), with a possible H_2 contribution below 1600 Å (Schwartz 1983; Böhm *et al.* 1987). It is not yet clear whether the departures from the two-photon

spectral shape below 1600 Å in the HH 2A' spectra are real or artifacts of the IUE response at very low exposure levels, and a calculation of the radiative dissociation ahead of the shock similar to that which we have performed for photoionization ahead of the shock will be needed to predict the H_2 emission. Therefore, we will defer analysis of the possible molecular emission for a future paper. Table 2 gives the integrated two-photon flux based on the theoretical two-photon spectral shape and the assumption that two-photon emission accounts for all the continuum flux in the 1700–1850 Å range, where

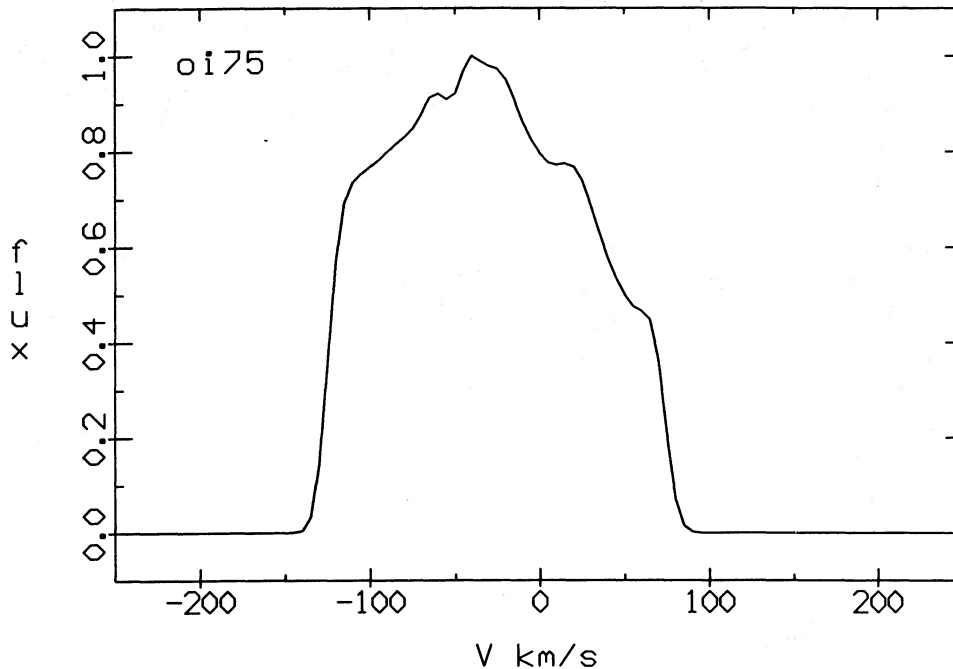


FIG. 2e

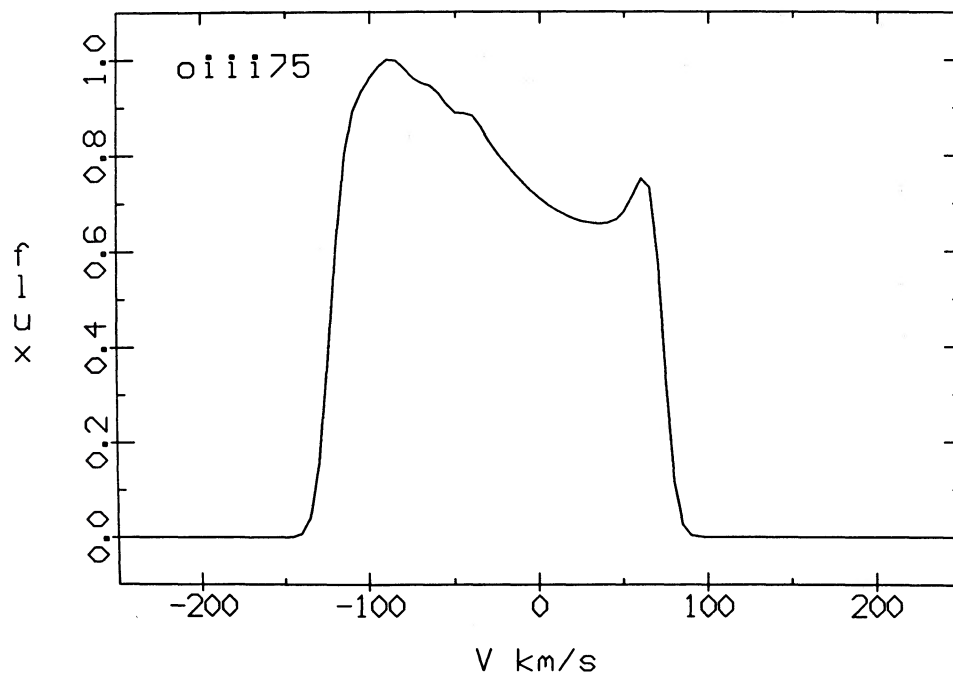


FIG. 2f

molecular emission should be unimportant. The continuum was measured from the spectrum of the central lines shown in Figure 3b.

IV. COMPARISON OF MODELS AND OBSERVATIONS

The profiles predicted by the present model have the same line widths and general shapes as those predicted by HRH. The major differences are that the neutral preshock gas near the bow shock tip increases the $H\alpha$ produced by collisional excitation at high velocities, and the partially ionized hydrogen at

low v_{eff} increases the $H\alpha$ recombination in the bow shock wings, near zero velocity. Thus the new profiles are less "boxy" and more "pointed" than the earlier ones, and they tend to agree better with the observed profiles of knots in HH 1 and HH 2 (see Hartmann and Raymond 1984). The qualitative differences between the [O III] profile shape and the shapes of lower excitation lines are not affected.

The optical emission-line fluxes predicted by the new model are generally closer to the observed line ratios than were those of HRH model 5, but the improvements are typically within

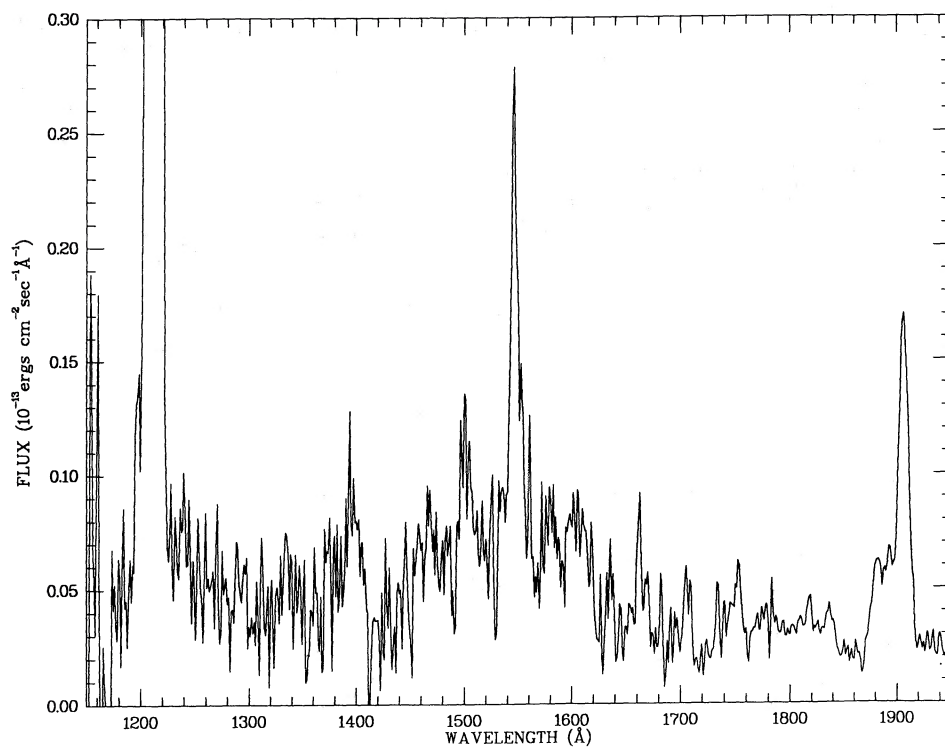


FIG. 3a

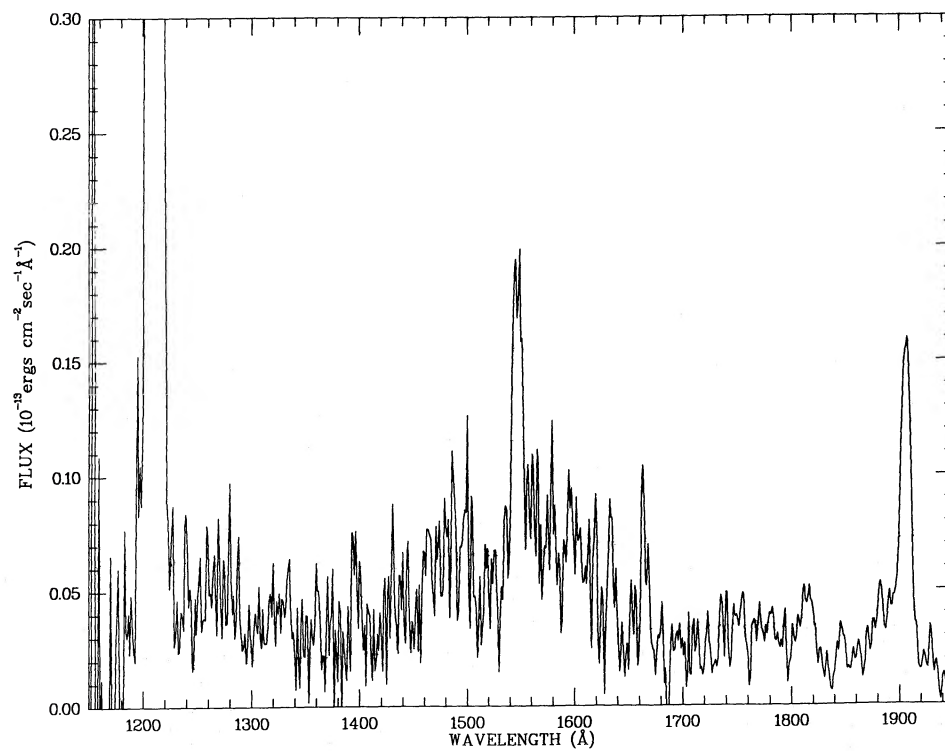


FIG. 3b

FIG. 3.—(a) Standard IUESIPS reduction of the HH 2A' IUE spectra. (b) IUE spectrum of the central portion of the large aperture obtained from the line-by-line data.

both observational and modeling uncertainties. The $[\text{O III}]/\text{H}\beta$ ratio predicted by the model is about 50% too large, which is a slight improvement over the previous model, and quite good agreement considering the approximate nature of the models. The largest discrepancy is for $[\text{C I}] \lambda 9849$, which is predicted to be 5 times brighter than observed. It is conceivable that this represents depletion onto grains. There is no evidence for depletion from the ultraviolet carbon lines, but $[\text{C I}]$ emission is suppressed at the high electron densities in the high v_{eff} parts of the flow which produce the UV lines. Models of grain destruction (Draine and Salpeter 1979; Seab and Shull 1983) show that carbon is effectively liberated from grains in shocks faster than about 100 km s^{-1} , and one might even attribute the modest difference between observed and predicted $\text{C IV}/\text{C III}$ ratios to progressive sputtering of grains in the shocked gas. This would be consistent with a normal carbon abundance derived from the UV lines and a substantial depletion of carbon inferred from the $[\text{C I}]$ line formed in the low v_{eff} bow shock wings. The $[\text{C I}]$ predictions are quite uncertain, however, and the neglect of molecular cooling in the models makes the lower temperature emission regions suspect.

The UV emission lines are difficult to assess, because of the uncertain relative normalization of the optical and UV emission and the reddening uncertainty. If the θ^2 reddening correction is appropriate, or if $E(B-V) = 0.11$, the observed and predicted C IV agree very well, while the C III line is half again as strong as predicted. We note that while resonant scattering within the emitting region severely reduces the C IV intensity observed from bright filaments of supernova remnants (Raymond *et al.* 1981, 1987), there should be no reduction in the C IV intensity from a cylindrically symmetric HH object, though the line profile would be modified and the very center of the profile subject to interstellar absorption. The other UV lines are too uncertain to be of use. If the color excess is 0.37 and an average reddening law is assumed, the observed fluxes are 3 or 4 times brighter than the model predictions. If we use the $\text{H}\beta$ flux given by Brugel, Böhm, and Mannery (1981), the UV lines are stronger than predicted by an additional factor of 2. Thus we conclude that the model is consistent with the observed fluxes, but the uncertainties in the reddening corrections preclude any real interpretation beyond the fact that the existence of any C IV emission at all requires a much higher shock velocity than would have been inferred from the optical spectrum alone.

The new model predicts a healthy hydrogen two-photon flux, and the ratio of the predicted continuum to $\text{H}\beta$ is similar to that which is typically observed in supernova remnants (Raymond *et al.* 1981, 1987). Unfortunately, it falls short of the continuum observed in HH 2A' by about a factor of 3. The IUE images show significant continuum emission filling the Large Aperture, but the continuum is clearly brightest in the same region where the emission lines are bright, and we have excluded about half the Large Aperture by using the line-by-line files. Judging from the contrast in continuum levels between the line-emitting region and the region free of line emission, it is likely that the continuum flux listed in Table 1 is still contaminated by continuum not associated with HH 2A', and this could reduce the two-photon fluxes listed in the table by about 50%. This leaves a factor of 1.5 discrepancy, which is within the uncertainties in the ratio of UV to optical emission.

If the two-photon emission actually is brighter than the model predictions, it is interesting to ask whether this anomaly is related to another difficulty with hydrogen. The $\text{H}\alpha/\text{H}\beta$ ratio

is between 4 and 5.5, depending on the reddening, while the models predict 3. The models would predict larger $\text{H}\alpha/\text{H}\beta$ ratios if the excitation occurred at temperatures below 50,000 K, but most of the hydrogen excitation in the models occurs in the fairly high v_{eff} region at temperatures above 10^5 K. All these models are based on the assumption of equal electron and ion temperatures, however, and Ohtani (1980) has shown that if plasma turbulence does not equilibrate electrons and ions rapidly, then the drastic cooling of the electrons by Lyman line excitation keeps the electron temperature low until most of the hydrogen is ionized. Thus a model with unequal electron and ion temperatures would give a steeper Balmer decrement, and it would give a two-photon/ $\text{H}\beta$ enhancement corresponding to the difference in excitation potentials. Dopita *et al.* (1986) have computed a model for a 45 km s^{-1} shock in neutral gas without electron-ion equilibration by plasma processes, and they find a two-photon/ $\text{H}\beta$ ratio 1.5–2 times the observed values listed in Table 2, so a bow shock model including a range of shock velocities and preshock ionization states might well produce strong enough two-photon emission.

The simple bow shock model predicts that the full width at zero intensity of all the lines should be the same and equal to the bow shock velocity (HRH). The bow shock velocities derived by HRH for HH 2A' were 160 km s^{-1} from the low-excitation ions, 204 km s^{-1} from $\text{H}\alpha$, and 254 km s^{-1} from $[\text{O III}]$. The systematic differences in line widths, and therefore in inferred bow shock velocities, between $[\text{O I}]$ and $[\text{S II}]$, $\text{H}\alpha$, and $[\text{O III}]$ are not explained by the new models, since preionization by itself does not affect the geometry of the bow shock. Excitation of neutral hydrogen entering the shock is the only major feature of the new models which might affect this discrepancy. Models of the emission from nonradiative shocks (Chevalier and Raymond 1978; Raymond *et al.* 1983) show that charge transfer creates a population of neutral H atoms having the thermal velocity distribution of the gas temperature just behind the shock. About half the Balmer emission produced by these neutrals emerges with a line width about equal to v_{eff} . In the 200 km s^{-1} bow shock model, about one-third of the $\text{H}\alpha$ emission from shocks faster than 100 km s^{-1} comes from excitation of the entering neutrals, and this accounts for 10% or 20% of the total $\text{H}\alpha$ emission. Thus about 10% of the $\text{H}\alpha$ emission has a 150 km s^{-1} wide thermal profile in addition to the bulk velocity included in the model profile calculation. This additional velocity width was not included in the model profile calculation shown in Figure 2. Taken together with the difficulty in measuring the faint high-velocity tails in the lower signal-to-noise $[\text{S II}]$ and $[\text{O I}]$ profiles, this probably accounts for the discrepancy between the bow shock velocities derived from $\text{H}\alpha$ and the low-excitation lines. This does not alleviate the discrepancy between $\text{H}\alpha$ and $[\text{O III}]$, however, and this discrepancy may reflect a breakdown of the assumption that the cooling length of the shocked gas is small compared with the bow shock size. Hydrodynamic calculations by Raga (1986) show that all the streamlines in the shocked gas curve toward the axis, so that lines emitted by relatively cool gas farther downstream will be narrower than lines emitted by hotter gas close to the shock.

While the differing widths of high- and low-excitation lines are common to many HH objects knots (HRH), the profiles of HH 2A' show much stronger asymmetry than the other knots in HH 1 and HH 2, and they tail off gradually on the negative velocity side. Figure 4 shows the $\text{H}\alpha$ profile presented by Hartmann and Raymond (1984) and an $[\text{O I}]$ profile obtained more

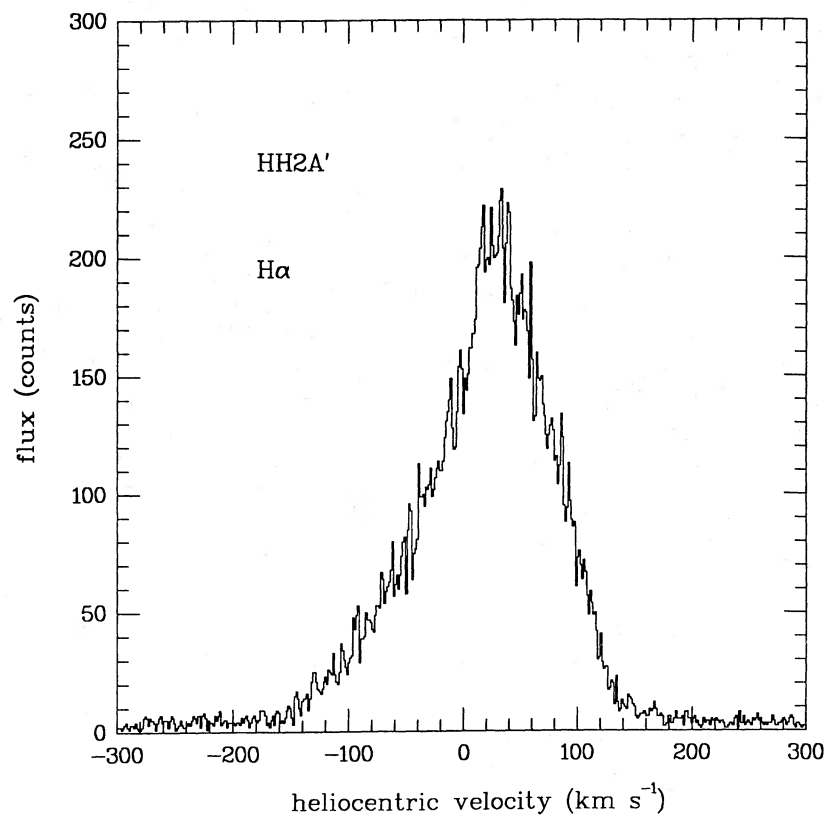


FIG. 4a

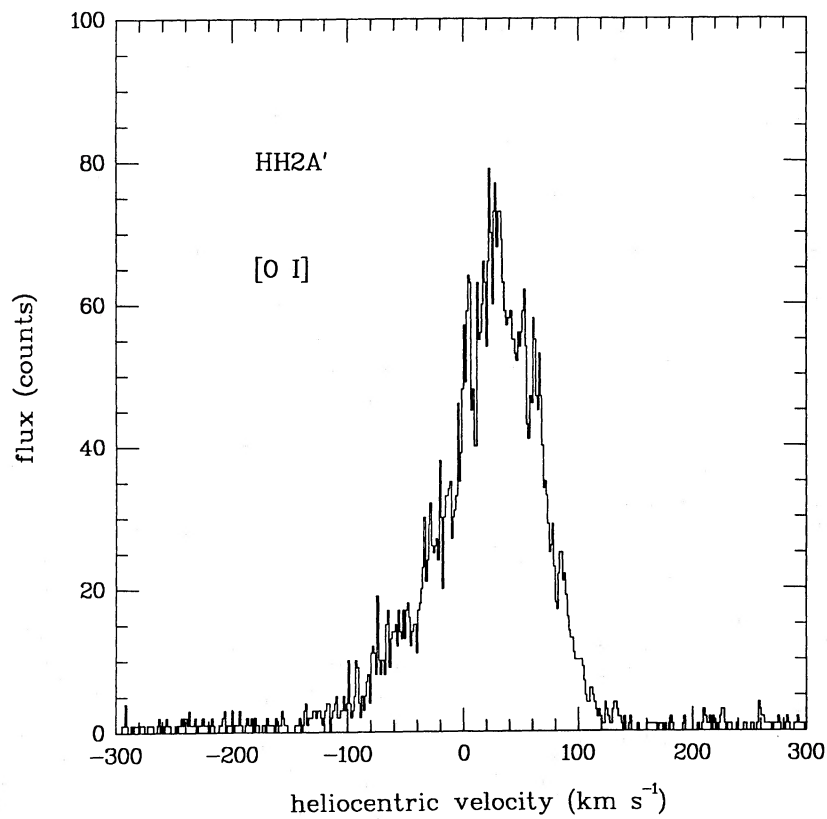


FIG. 4b

FIG. 4.—(a) H α profile of HH 2A' from Hartmann and Raymond (1984). (b) HH 2A' [O I] line profile.

recently with the same instrument on the MMT. While a bow shock moving at an angle to the line of sight can produce asymmetric profiles, it is hard to explain the asymmetry together with the peaking of the profile near zero velocity. Therefore, the unique profiles of HH 2A' may indicate a breakdown of the cylindrical symmetry assumed in the models. This could reflect either an asymmetric cloud driving the bow shock or a density gradient in the preshock medium with a significant change in density over the bow shock scale of 10^{16} cm. In either case, the fact that this marked asymmetry occurs in the HH object knot which has most recently appeared (Herbig and Jones 1981) suggests that the bow shocks tend to become more symmetric fairly rapidly.

We conclude that departures from equilibrium preionization do not drastically affect either the line profiles or the predicted relative line intensities of a 200 km s^{-1} bow shock, though the effects that are predicted tend to be in the sense that improves the agreement with observation. The effects will be much more severe for slower bow shocks. From Figure 1 it is apparent that a bow shock slower than 150 km s^{-1} will encounter almost entirely neutral gas. Therefore a 100 or 120 km s^{-1} bow shock would produce almost no [O III] emission, and the spectrum of such a bow shock would resemble a very slow planar shock. This could resolve the discrepancy between the bow shock velocities inferred from the line widths of HH 7-11 and the very low excitation spectra (HRH), especially when cooling by H_2 is included in the models.

V. SUMMARY

While the bow shock models successfully account for the major features of HH object emission, it is worthwhile to repeat the limitations of the models and the discrepancies between the models and observations, and to ask which features of the bow shock models are really essential to explaining the observations.

The most important limitations of the models are the

assumption of a round cloudlet, the assumption that the bow shock can be approximated by a set of steady state, plane-parallel oblique shocks (a good approximation only if the cooling distance is small compared with the overall scale of the bow shock), and the neglect of thermal instabilities at high v_{eff} (Innes, Giddings, and Falle 1986; Raga and Böhm 1987). The major discrepancies between the models and the observations are the differing [O III] and $\text{H}\alpha$ line widths (though the qualitative difference between their shapes is correctly predicted), and perhaps the [O III]/ $\text{H}\beta$ ratios which are predicted to be larger than observed for the bow shock velocity which matches the line widths. While the bow shock models were inspired by ideas of stellar winds striking dense clouds (Schwartz 1978) or dense clouds plowing through the ambient gas at high speed (Norman and Silk 1979), the observations do not provide direct evidence for the dense clouds themselves. The essential feature of the bow shock models which provides both the broad range in effective shock velocities needed to reproduce the emission-line spectrum and the range in projected velocity needed to match the line profiles is the very strong curvature of the shock front. Azimuthal symmetry may not be essential, but it certainly provides a natural explanation for the general shapes of the profiles and the agreement between the line widths and the bow shock velocity needed to produce the ultraviolet emission. The normal component of the shock velocity must vary over more than a factor of 4 to give both strong [N I] and strong C IV, and the radius of curvature must be less than about 10^{16} cm in HH 2A'. Detection of the cloud itself, most probably at radio wavelengths, is crucial to further understanding of these objects.

We thank the staff of the IUE satellite for their support in the acquisition of these data, and G. Nassiopulos for help in reducing the data. This work was supported by National Aeronautics and Space Administration grant NAS5-87 to the Smithsonian Astrophysical Observatory.

REFERENCES

- Böhm, K.-H., Böhm-Vitense, E., and Cardelli, J. A. 1982, in *Advances in Ultraviolet Astronomy*, ed. Y. Kondo, J. M. Meade, and R. D. Chapman (NASA CP 2238), p. 223.
- Böhm, K.-H., Bürke, Th., Raga, A. C., Brugel, E. W., Witt, A. N., and Mundt, R. 1987, *Ap. J.*, **316**, 349.
- Bohlin, R. C., and Savage, B. D. 1981, *Ap. J.*, **249**, 109.
- Brugel, E. W., Böhm, K.-H., and Mannery, E. 1981, *Ap. J. Suppl.*, **47**, 117.
- Brugel, E. W., Shull, J. M., and Seab, G. C. 1982, *Ap. J. (Letters)*, **262**, L35.
- Chevalier, R. A., and Raymond, J. C. 1978, *Ap. J. (Letters)*, **225**, L27.
- Choe, S.-U., Böhm, K.-H., and Solf, J. 1985, *Ap. J.*, **288**, 338.
- Cox, D. P. 1972, *Ap. J.*, **178**, 143.
- Cox, D. P., and Raymond, J. C. 1985, *Ap. J.*, **298**, 651.
- Dopita, M. A. 1978, *Ap. J. Suppl.*, **37**, 117.
- Dopita, M. A., Binette, L., and Schwartz, R. D. 1982, *Ap. J.*, **261**, 183.
- Dopita, M. A., Caganoff, S., Schwartz, R. D., and Cohen, M. 1986, in *IAU Symposium 115, Star Forming Regions*, ed. M. Peimbert and J. Jugaku (Dordrecht: Reidel), p. 346.
- Draine, B. T., and Salpeter, E. E. 1979, *Ap. J.*, **231**, 438.
- Hartigan, P., Raymond, J., and Hartmann, L. 1987, *Ap. J.*, **316**, 323 (HRH).
- Hartmann, L., and Raymond, J. C. 1984, *Ap. J.*, **276**, 560.
- Herbig, G. H., and Jones, B. F. 1981, *A. J.*, **86**, 1232.
- Innes, D. E., Giddings, J. R., and Falle, S.A.E.G. 1986, in *Proc. Workshop on Model Nebulae*, ed. D. Péquignot (Observatoire de Paris), p. 153.
- Norman, C., and Silk, J. 1979, *Ap. J.*, **228**, 197.
- Ohtani, H. 1980, *Pub. Astr. Soc. Japan*, **32**, 11.
- Ortolani, S., and D'Odorico, S. 1980, *Astr. Ap.*, **83**, 68.
- Raga, A. C. 1986, Ph.D. thesis, University of Washington.
- Raga, A. C., and Böhm, K.-H. 1985, *Ap. J. Suppl.*, **58**, 201.
- . 1987, preprint.
- Raymond, J. C. 1979, *Ap. J. Suppl.*, **39**, 1.
- Raymond, J. C., Black, J. H., Dupree, A. K., Hartmann, L., and Wolff, R. S. 1981, *Ap. J.*, **246**, 100.
- Raymond, J. C., Blair, W. P., Fesen, R. A., and Gull, T. R., Jr. 1983, *Ap. J.*, **275**, 636.
- Raymond, J. C., Hester, J. J., Cox, D., Blair, W. P., Fesen, R. A., and Gull, T. R. 1987, *Ap. J.*, **324**, 869.
- Schwartz, R. D. 1975, *Ap. J.*, **195**, 631.
- . 1978, *Ap. J.*, **223**, 884.
- . 1983, *Ap. J. (Letters)*, **268**, L37.
- Seab, C. G., and Shull, J. M. 1983, *Ap. J.*, **275**, 652.
- Shull, J. M., and McKee, C. F. 1979, *Ap. J.*, **227**, 131.

P. HARTIGAN, L. HARTMANN, and J. RAYMOND: Harvard-Smithsonian Center for Astrophysics, 60 Garden Street, Cambridge, MA 02138